Structure of a lipid-bound viral membrane assembly protein reveals a modality for enclosing the lipid bilayer

Prabhat Kumar Pathak[a,1], Shuxia Peng[a,1], Xiangzhi Meng[b,1], Yue Han[a], Bing Zhang[a], Fushun Zhang[b], Yan Xiang[b,2], and Junpeng Deng[a,2]

[a]Department of Biochemistry and Molecular Biology, Oklahoma State University, Stillwater, OK 74078; and [b]Department of Microbiology, Immunology, and Molecular Genetics, University of Texas Health Science Center at San Antonio, San Antonio, TX 78229

Edited by Wesley I. Sundquist, University of Utah School of Medicine, Salt Lake City, UT, and approved May 25, 2018 (received for review April 4, 2018)

Cellular membranes are maintained as closed compartments, broken up only transiently during membrane reorganization or lipid transportation. However, open-ended membranes, likely derived from scissions of the endoplasmic reticulum, persist in vaccinia virus-infected cells during the assembly of the viral envelope. A group of viral membrane assembly proteins (VMAPs) were identified as essential for this process. To understand the mechanism of VMAPs, we determined the 2.2-Å crystal structure of the largest member, named A6, which is a soluble protein with two distinct domains. The structure of A6 displays a novel protein fold composed mainly of alpha helices. The larger C-terminal domain forms a unique cage that encloses multiple glycerophospholipids with a lipid bilayer-like configuration. The smaller N-terminal domain does not bind lipid but negatively affects lipid binding by A6. Mutations of key hydrophobic residues lining the lipid-binding cage disrupt lipid binding and abolish viral replication. Our results reveal a protein modality for enclosing the lipid bilayer and provide molecular insight into a viral machinery involved in generating and/or stabilizing open-ended membranes.

vaccinia A6 | crystal structure | crescent membrane | nonvesicular transfer | VMAP

Eukaryotic cells are compartmentalized by biological membranes, which are maintained as closed-end structures in the cytosol (1). To allow intracellular trafficking, the membranes have to undergo fission and fusion, which are orchestrated by dedicated cellular protein machineries (2–4). These processes are highly coordinated, so the breach in the membrane bilayers is usually transient. In contrast, open-ended membranes persist in vaccinia virus-infected cells during the assembly of the primary envelope of the virus, offering a unique opportunity for studying the molecular mechanism of membrane reorganization. Vaccinia virus (VACV) is the best-studied poxvirus, a family of complex DNA viruses that replicate in the cytoplasm of infected cells (5). Compared with many other viruses, poxvirus replication is relatively autonomous, relying on virus-encoded machineries for many essential processes such as gene transcription, genome replication, and virus assembly (5). While most enveloped viruses obtain their envelope by budding, a process that is similar to the formation of cellular transport vesicles, poxviruses acquire their primary envelope through extending of open-ended, crescent membranes (6, 7). The origin and biogenesis of the crescent membranes have puzzled virologists for over half a century, although recent studies suggest that the crescents derive from rupture of the endoplasmic reticulum (ER) (8, 9). Five viral proteins, A6, A11, A30.5, H7, and L2, have been found to be essential for crescent membrane formation. They are conserved in all vertebrate poxviruses and collectively are termed viral membrane assembly proteins (VMAPs) (7). VMAPs are thought to be involved in generating and/or stabilizing scission of ER membranes (8), but there is no molecular evidence that supports such a role for any of the VMAPs.

Among the VMAPs, all but A6 have a known connection to membranes or lipids. L2 (10 kDa) and A30.5 (4.8 kDa) are small transmembrane proteins that form a tight complex and colocalize to the ER (10). H7 is a 17-kDa cytoplasmic protein that binds phosphoinositol (11). A11, a 36-kDa protein, does not associate with membranes in uninfected cells but associates exclusively with viral membranes in vaccinia virus-infected cells (12, 13). A6 is the largest VMAP (43 kDa) with two separate domains (14) and localizes predominantly in the cytosol (15, 16). In this study, we determined the crystal structures of the N-terminal domain of VACV A6 and the C-terminal domain of an A6 ortholog from fowlpox virus. Our structural and functional studies of A6 reveal a unique protein modality for interacting with the lipid bilayer and provide molecular insight into how VMAPs could facilitate the generation and stabilization of the open-ended membrane sheets.

Results

The Structures of A6 Orthologs. To gain a structural insight into the function of VACV A6, we first expressed and purified full-length (FL) A6 from *Escherichia coli*. Although FL A6 crystalized, the crystals did not diffract, possibly due to conformational heterogeneity.

Significance

Cellular membranes are maintained as closed structures in the cytosol, and any breaches in membranes during reorganization are transient. However, open-ended membranes, likely derived from the endoplasmic reticulum, persist in vaccinia virus-infected cells during the assembly of the vaccinia envelope. A group of viral proteins have been identified to be required for this process, providing a unique opportunity for dissecting the molecular mechanism of membrane scission and remodeling. Our structural and functional studies of one of these viral proteins reveal a cage-like soluble protein that traps internally multiple lipids with a bilayer-like configuration. Our studies reveal a protein modality for enclosing the lipid bilayer and suggest a mechanism for stabilizing the open-ended membrane sheets.

Author contributions: Y.X. and J.D. designed research; P.K.P., S.P., X.M., Y.H., B.Z., and F.Z. performed research; Y.X. and J.D. analyzed data; and Y.X. and J.D. wrote the paper.

The authors declare no conflict of interest.

This article is a PNAS Direct Submission.

Published under the PNAS license.

Data deposition: Atomic coordinates and structure factors have been deposited with the Protein Data Bank, https://www.rcsb.org, with accession codes 6CB6, 6CB7, 6BR8, and 6BR9.

[1]P.K.P., S.P., and X.M. contributed equally to this work.

[2]To whom correspondence may be addressed. Email: xiangy@uthscsa.edu or junpeng.deng@okstate.edu.

This article contains supporting information online at www.pnas.org/lookup/suppl/doi:10.1073/pnas.1805855115/-/DCSupplemental.

Published online June 18, 2018.

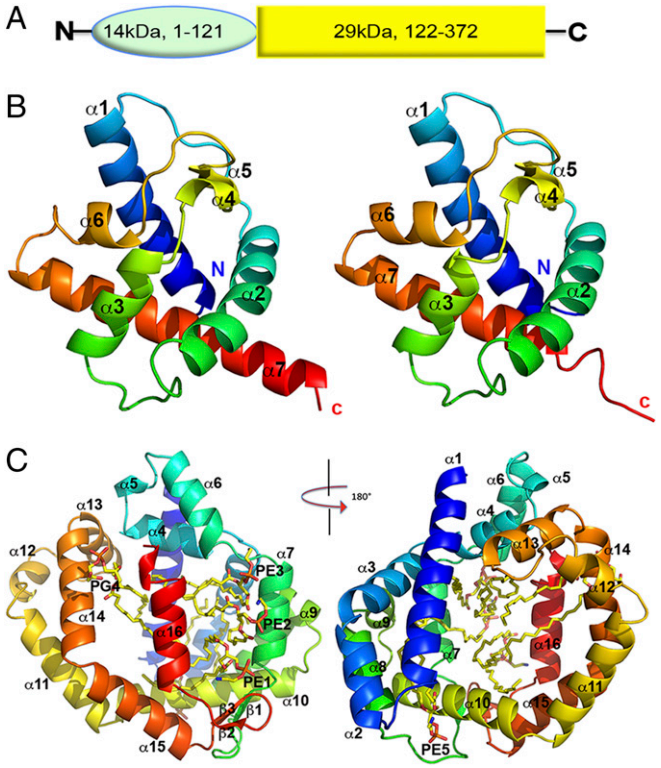

Fig. 1. The structures of A6 orthologs. (*A*) VACV A6 domain architecture. The 14-kDa N-domain and the 29-kDa C-domain of A6 are shown in green and yellow, respectively. (*B*) The structures of VACV A6-N in two space groups: (*Left*) C2, (*Right*) $P4_12_12$. Note the unwinding of the C terminus in $P4_12_12$. (*C*) The structure of the FPV170-C domain (space group $P2_12_12_1$). The secondary structures are labeled and colored with the N terminus in blue and the C terminus in red. The glycerophospholipids are shown as stick models.

As we previously identified a two-domain architecture for A6 through limited proteolysis analysis (Fig. 1*A*) (14), we then pursued the structures of the individual domains. We expressed and purified the N-terminal domain of 121 amino acids and the C-terminal domain of 251 amino acids. Both domains crystalized but failed to diffract. After protein surface engineering (*Materials and Methods*), the N-domain crystals diffracted to 1.6-Å high resolution. We then tested the C-domain of A6 orthologs from several other poxviruses and found the one from fowlpox virus (FPV170) forming diffractable crystals. The amino acid sequences of A6 and FPV170 share 58% similarity.

The N-domain of A6 (A6-N) crystallized in two space groups, yielding two nearly identical structures with a root mean square deviation (rmsd) of 0.27 Å over 101 aligned Cα atoms. The structures are compact with an overall dimension of ∼40 Å × 39 Å × 30 Å. They comprise mainly of seven α-helices connected with loops of varying length (Fig. 1*B*). The helices α1, α2, and α7 are significantly longer than the others. The main difference between the structures from the two different space groups lies at the C-terminal end (residue 114–119), which adopts an α-helix in one crystal form (C2, Fig. 1*B*, *Left*) but unwinds to a coil in the other ($P4_12_12$). This conformational difference suggests that the region connecting the N- and C-domains is dynamic.

The C-domain of FPV170 (FPV170-C) also crystallized in two space groups, having either one ($C222_1$) or two ($P2_12_12_1$) molecules in the asymmetric unit (ASU). The crystals diffracted up to 2.2 Å resolution, yielding nearly identical structures. The pairwise rmsd values between the monomer in the ASU of $C222_1$ and the two molecules in the $P2_12_12_1$ are 0.68 Å and 0.8 Å over 230 aligned Cα atoms, respectively. The rmsd between the two molecules in the ASU of $P2_12_12_1$ is 0.41 Å over 249 aligned Cα atoms. The structures in $P2_12_12_1$ contain all of the residues except the first two, while the structure in $C222_1$ has two disordered loops (amino acids 147–156 connecting α1 and α2, and 229–233 connecting β1 and α8). The structures comprise 16 α-helices and a very short three-stranded antiparallel β-sheet, with varying lengths of loops connecting the secondary structures (Fig. 1*C*). The overall structure forms a large "cage" with no internal amino acids. A structure similarity search using the Secondary Structure Matching server (17) and the DALI server (18) did not yield any significant match to either N- or C-domain structure, suggesting that A6 adopts a novel protein fold.

FPV170-C Binds Multiple Glycerophospholipids with a Lipid Bilayer-Like Configuration. Strikingly, we found clearly interpretable electron densities within the cage of FPV170-C that could be modeled as glycerophospholipids (Figs. 1*C* and 2 and *SI Appendix*, Fig. S1 and Table S1). To identify the lipid molecules, we extracted the lipids from the purified FPV170-C and performed a lipidomic profiling analysis (*Materials and Methods*). Mass spectrometry identified two major glycerophospholipid components, phosphatidylethanolamine (PE, 56.5%) and phosphatidylglycerol (PG, 42.5%), which are major components of *E. coli* cellular membranes. The lipids had either 33 or 34 carbons in the bifurcated tails (*SI Appendix*, Fig. S2). At the current resolution of the structure, we could not precisely define the number of lipid carbons, but all of the lipids can be modeled as PE or PG with 34 carbon side chains (16:0, 18:1) with good refinement statistics (*SI Appendix*, Table S1).

We located five lipids in each of the crystal forms. Among the five observed lipids, four (PE1, PE2, PE3, PG4) occupy similar positions in both crystal forms and superimpose well, while the fifth lipid (PE5a or PE5b) locates differently in the two crystal forms (Fig. 2 and *SI Appendix*, Fig. S1). Since PE5a and PE5b do not overlap, FPV170-C could bind six glycerophospholipids when fully saturated (*SI Appendix*, Fig. S3). The distance between the phosphate groups of PE1 and PE5b in $P2_12_12_1$ is about 30 Å, and the acyl polycarbon chains of all lipids make up an exclusively hydrophobic layer of about 26 Å in depth. The observed configuration of the lipids resembles that from a

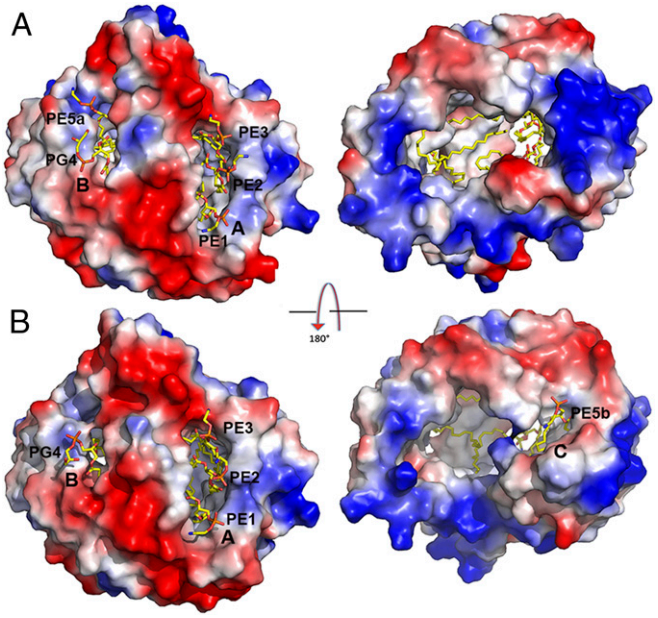

Fig. 2. The structure of the FPV170-C reveals a novel lipid-binding fold. The electrostatic surfaces of FPV170-C are shown in *A* (space group $C222_1$) and *B* (space group $P2_12_12_1$). Five glycerophospholipid molecules were observed including four PEs and one PG. The lipids are bound at three sites, labeled as A, B, and C. The glycerophospholipids are shown as stick models.

BIOCHEMISTRY

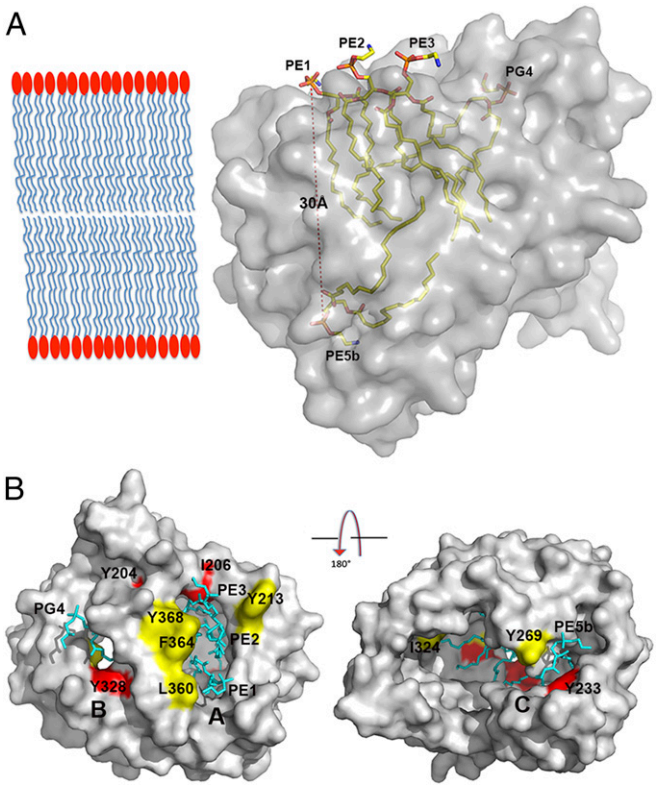

Fig. 3. FPV170-C traps lipids with a bilayer-like configuration. (*A*) The five glycerophospholipids (space group $P2_12_12_1$) are shown as sticks. The membrane bilayer is shown schematically with phosphate head groups shown as red and acyl lipid tails shown as blue wavy lines. The FPV170-C structure is shown as the gray surface. (*B*) Residues subjected to mutagenesis studies. The modeled VAVC-A6-C structure is shown as a gray surface. The substituted 10 residues are labeled and colored as red (essential) and yellow (nonessential), respectively. The bound lipids are shown as cyan sticks.

biological membrane bilayer, with PE1, PE2, PE3, PG4 in one leaflet and PE5b in the other (Fig. 3), tightly wrapped by the hydrophobic inner surface of the protein cage. A single soluble protein that traps multiple lipids with a lipid bilayer-like configuration has not been reported previously.

The glycerophospholipids contact the FPV170-C protein predominantly through hydrophobic interactions via acyl lipid tails and the greasy inner surface of the protein cage. The phosphate head groups of the lipids are all solvent-exposed, making minimum contact with the protein and suggesting that A6 binds glycerophospholipids without any preferences for the head groups. We name the locations of the protein where the lipids are bound as sites A, B, and C (Fig. 2 and *SI Appendix*, Fig. S1). Site A is a hydrophobic groove sandwiched between helices α5, α6, β1, β2, and α14, containing three PE molecules (PE1, PE2, and PE3) in both crystal forms. Site B locates between helices α3, α4, α12, α13, and α14, containing two glycerophospholipids in one crystal form (PG4 and PE5a in $C222_1$) but only one in the other (PG4 in $P2_12_12_1$). PE5a is situated in a hydrophobic groove composed of helices α3, α4, α12, and the beginning of α13. Site C is sandwiched by helices α1, α2, α7, and α9 and contains a PE molecule (PE5b) only in the $P2_12_12_1$ structure.

Lipid Binding by A6 Is Modulated by A6-N. To further study the binding of glycerophospholipids by A6, we developed a lipid-binding assay with a fluorescence-labeled lipid, 7-nitrobenz-2-oxa-1,3-diazol-4-yl-1,2-dipalmitoyl-sn-glycero-3-phosphoethanolamine (NBD-PE) (*SI Appendix*, Fig. S4). On a native polyacrylamide gel electrophoresis (PAGE), NBD-PE comigrated with A6-C, resulting in a strong fluorescence signal for the protein band. In contrast, NBD-PE did not comigrate with A6-N (*SI Appendix*, Fig. S4, lane 1), indicating A6-N does not bind lipids. Interestingly, the fluorescence signal associated with FL A6 was only about 22% of that with A6-C, indicating a reduced lipid binding by the FL protein (*SI Appendix*, Fig. S4). A similar reduction in lipid binding was also observed for FL FPV170 in comparison with FPV170-C (*SI Appendix*, Fig. S4), suggesting that the N-domain of A6 orthologs modulates lipid binding by the C-domain. However, adding purified A6-N to A6-C did not cause significant change in lipid binding.

Lipid Binding by A6 Is Essential for Viral Replication. Based on the FPV170-C structure, we created a homology model of the A6-C structure. We then selected 10 hydrophobic residues that are in close proximity with the acyl lipid tails at the three binding sites for alanine substitution. To evaluate the effect of the mutations on lipid binding, we purified all 10 A6 mutant proteins from *E. coli* and tested their binding of NBD-PE on native PAGE. Compared with WT A6-C, four mutants—Y204A (site A), I206A (site A), Y328A (site B) and Y233A (site C)—displayed a substantial decrease in lipid binding (Fig. 4 and *SI Appendix*, Fig. S5). Notably, these four residues are mostly conserved among poxvirus orthologs (*SI Appendix*, Fig. S6). Circular Dichrosim analysis of the mutant proteins revealed no change with respect to WT protein, indicating that the mutations did not change the overall protein structure. The 10 mutations were also introduced individually into the A6 gene of VACV, and the same four mutations were found to cause severe defects in viral replications. Y233A resulted in greatly reduced viral yield, while Y204A, I206A, and Y328A had a lethal effect on viral replication (Fig. 5 and *SI Appendix*, Fig. S7). Our data indicate that the lipid binding by A6 is vital for its function in viral replication.

Discussion

Due to the hydrophobic nature of the acyl lipid tails, cellular membranes are maintained as closed structures in the aqueous cytosol, and any breaches in membranes during reorganization are transient. However, stable open-ended membranes, named

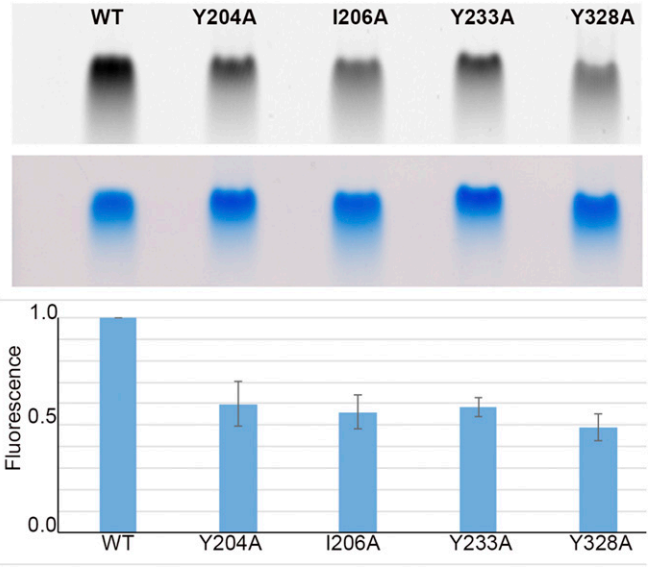

Fig. 4. Mutations of lipid-binding sites of A6 reduce lipid binding. The fluorescence scans of the native PAGE with WT and mutant VACV-A6-C proteins in the presence of NBD-PE is shown on the *Top*. The Coomassie stain of the same gel is shown in the *Middle*. The normalized fluorescence signals are presented as mean ± SEM ($n = 3$). Significance was found between A6 WT and mutants by two-tailed *t* test ($P = 0.015$, 0.007, 0.010, and 0.004 for Y204A, I206A, Y233A, and Y328A, respectively).

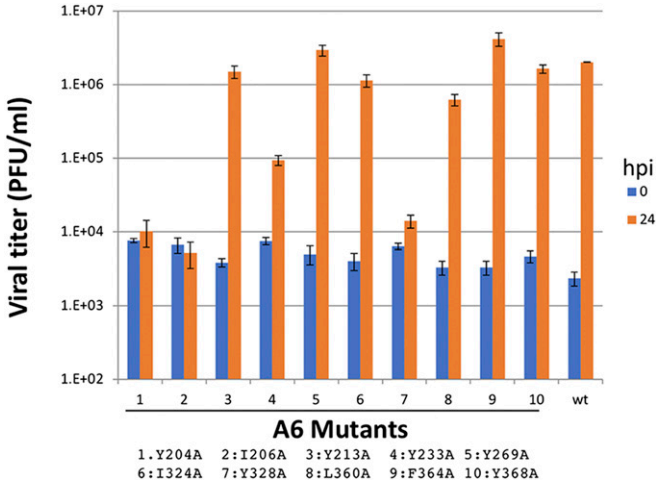

Fig. 5. Mutations of lipid-binding sites of A6 cause defects in viral replication. BSC-1 cells in 12-well plates were infected with the indicated viruses. Viral titers at 0 and 24 h hpi were determined by plaque assay on an A6-expressing cell line.

crescent membranes, persist in vaccinia virus-infected cells during the assembly of the viral envelope (7, 9). The crescent membranes are likely derived from scissions of the ER membranes (8, 9), and a defined group of viral membrane assembly proteins (VMAPs) are required for this process. The study of the protein machinery involved in VACV envelope assembly therefore provides a unique opportunity for dissecting the molecular mechanism of membrane scission and remodeling. The sustained existence of open-ended crescents provides an unusually long window of opportunity for capturing the machinery in action, and the ease of viral genetics allows facile manipulation of the machinery. VMAPs are believed to be involved in generating and/or stabilizing the open-ended crescent membranes (8, 9). However, there is no direct evidence to support such a role. In this study, we have determined the crystal structures of the A6 protein, which is the largest VMAP. The A6 structure reveals a novel protein fold with an unprecedented large lipid-binding capacity. Most strikingly, the lipids bound by A6 display a molecular geometry that is similar to the biological membrane bilayer. In contrast to integral membrane proteins that make contacts with the bilayer through the surface of a transmembrane domain, A6 wraps around and shields the bilayer from solvent. One of the best-characterized families of soluble proteins that carry lipids internally are the lipid transfer proteins (LTP) (19). However, A6 differs drastically from any of the known LTPs in not only protein folding but also lipid-binding capacity. All known LTPs to date predominantly adopt a conserved beta–barrel-like protein fold that binds a single molecule of lipid, while A6 is mainly alpha helical and traps likely six but at least five glycerophospholipids (*SI Appendix*, Fig. S3). To our knowledge, this is the first time a single soluble protein was observed to interact with lipids with a bilayer-like configuration.

Complementary to the crystallographic observations, the lipidomic profiling by MS analysis and the in vitro lipid-binding assay confirmed that A6 is a lipid-binding protein. An in vivo viral replication assay showed that the lipid binding by A6 is essential for viral replication. Our structural and functional analysis demonstrated that the two domains have distinct functions. In contrast to the lipid-binding C-domain, the compact N-domain does not bind lipids but decreases the lipid binding by the C-domain, as FL A6 displayed much weaker NBD-PE binding in our in vitro assays. This could occur through allosteric effects from interdomain associations or through the N-domain–mediated protein–protein interactions with other VMAPs. The C-terminal end of the A6 N-domain displays different conformations in the two different crystal forms (Fig. 1*B*), suggesting a dynamic connection between the two domains. In addition, all FL A6 orthologs that we examined either failed to crystallize or the crystals could not diffract, suggesting that the proteins are intrinsically dynamic. This structural dynamic may be essential for regulating lipid binding by A6, and this regulation may be necessary in the control of the protein machinery for membrane remodeling.

The direct visualization of the captured lipid bilayer by A6 provides insights into how open-ended membranes could be stabilized during membrane scission. As illustrated by the model in Fig. 6, A6 could stabilize the open-ended membrane sheet by shielding away the aliphatic tails of the lipids from the aqueous environment. Since the ends of the membrane sheet may have to be exposed to allow the growth of the crescent membranes, the binding of A6 to the crescent membranes might be dynamic and modulated by transient interactions with other VMAPs. This could explain why A6 localizes predominately to the cytosol and only partially with the ER markers (13, 16). A6 was reported to have a weak interaction with A11 (12), which was shown to associate with the edges of crescent membranes and nearby ER membranes by immunogold transmission electron microscopy (13). L2 also associates with the edges of crescent membranes and forms a tight complex with A30.5, although no interactions between L2 and A30.5 with other VMAPs were detected (13). Another model for A6 function that is consistent with its structure is that it may act analogously to cellular LTPs to transfer lipids from the ER to the site of virion assembly. The difference in lipid binding between the C-domain and the FL A6 suggests that A6 may adopt at least two different conformations, a closed and an open state for binding and releasing glycerophospholipids. Again, a dynamic connection between the two domains and the interactions with other VMAPs may be important for regulating this activity of A6.

The molecular mechanism of how all VAMPs work in concert during this process is still unknown. Nevertheless, our structural and functional data provide fresh insights into the mechanisms of stabilization of open-ended membrane sheets generated from membrane scission and a potential nonvesicular lipid transfer during membrane biogenesis.

Materials and Methods

Protein Purification and Crystallization. VACV A6 and FPV170, as well as its N-domains (1–122 VACV A6) or C-domains (124–374 FPV170, 124–372 VACV A6) were individually cloned in a modified pET vector as a SUMO fusion with a N-terminal 6xHis-tag. The recombinant proteins were expressed in *E. coli* and purified by Ni-NTA as previously described (20). Briefly, the fusion proteins were first purified from soluble cell lysate using an Ni-NTA affinity column. The eluted protein was subsequently subjected to Ulp1 protease cleavage and was collected as flow-through of a second subtracting Ni-NTA column. The proteins were further purified by cation exchange and size-exclusion chromatography to homogeneity. The selenomethionine (SeMet) substituted proteins were

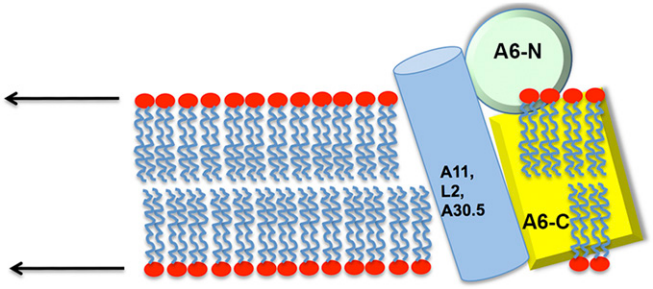

Fig. 6. A model for stabilization of an open-ended membrane sheet by VMAPs. The domain of A6 is shown and colored in the same scheme as in Fig. 1*A*. The membrane bilayer is depicted in the same scheme as in Fig. 3. VMAPs that potentially associate with A6 in the stabilization of open ends are shown as a blue cylinder. The open-ended sheet is stabilized by A6 through lipid binding and protein–protein interactions, shielding the hydrophobic acyl chains from aqueous environment.

BIOCHEMISTRY

expressed in M9 minimal medium supplemented with amino acids as described (21) and purified using procedures described above. The purified proteins were concentrated to 20 mg/mL in 10 mM sodium phosphate (pH 6.0), 150 mM NaCl, and 5 mM Tris(2-carboxyethyl)phosphine, flash-frozen, and stored at −80 °C until used (22). VACV A6-N protein crystals were obtained at 4° in a solution containing 4 M ammonium citrate (pH 7.0), which diffracted to only 8 Å. Residues E47, K48, and K49 were mutated to alanines to reduce surface entropy (23). This mutant protein crystallized under two different conditions, one with 15% polyethylene glycol (PEG) 3350 and 0.15 M cesium chloride, and the other with 20% PEG2000, 0.1 M Tris (pH 8.5). Two different crystal forms were obtained: $P4_12_12$ (1.6 Å) and C2 (1.8 Å). FPV170-C crystallized in two different space groups ($P2_12_12_1$ and $C222_1$), both in 0.2 M potassium thiocyanate and 30% PEG3350. For data collection, 20–35% glycerol was added to the mother liquid as cryoprotectant.

Structure Determination. All data were collected at the beamline 19-ID at the Advanced Photon Source, Argonne National Laboratory. The structures of VACV A6-N and FPV170-C were both solved by the Single-Wavelength-Anomalous-Dispersion method using program HKL3000 (24), with data collected from single SeMet-substituted protein crystals. A nearly complete model was constructed from the experimental phases obtained from the SeMet crystal data. This model was used to solve the native structures at higher resolution by the molecular replacement method using the program Phaser (25). The PHENIX program (26) was used for the refinement, and Coot (27) was used for the iterative manual model building. Translation, libration, and screw-rotation displacement groups used in the refinement were defined by the TLMSD server (28). The current models are of good geometry and refinement statistics (*SI Appendix*, Table S1). All molecular graphic figures were generated with PYMOL (29).

Lipid-Binding Assay. Purified A6 proteins (19 μL, ∼2 mg/mL) in 20 mM Tris (pH 8.0), 150 mM NaCl, and 10 mM DTT were mixed with 2 μL NBD-PE 16:0 at 1 mg/mL in methanol, incubated on ice for 1 h, and subsequently analyzed by native PAGE. A Typhoon Trio Variable mode Imager was used for the visualization of the fluorescence and Coomassie-stained protein bands from the gel.

Lipid Extraction and Lipidomic Profiling. Lipids were extracted from the recombinant FPV170-C protein that was used for crystallization. The protein solution was sonicated in chloroform/methanol/water (2:2:1 vol ratio) for 10 min. The mixture was centrifuged at 1,500 × *g* for 10 min to remove protein precipitates. The chloroform phase was removed by pasture pipette and washed with 0.5 mL 1 M KCL followed by 0.5 mL water. The collected chloroform phase containing lipids was vacuum-dried and sent to the Lipidomics Research Center at Kansas State University for lipid-profiling MS analysis. Phospholipids were analyzed by targeted electrospray ionization triple quadrupole mass spectrometry, using internal standards and precursor and neutral loss scans to measure molecular species of phosphatidylcholine, lysophosphatidylcholine, phosphatidylethanolamine, lysophosphatidylethanolamine, phosphatidylinositol, phosphatidylserine, phosphatidic acid, and phosphatidylglycerol, as described by Xiao et al. (30). A single sample was analyzed, and the mass spectral background observed from an identically analyzed sample with internal standards alone was subtracted from the experimental data.

Construction of VACV A6 Mutants. VACV with a deletion in A6L (vΔA6), HeLa cell lines inducibly expressing VACV A6 (HeLa-iA6), and a plasmid (pRY57) with the coding sequence for A6 with a C-terminal V5 epitope tag and GFP between the A7 and A5 sequence were described previously (14). VACVs expressing various mutant A6Ls were constructed by homologous recombination of vΔA6 with derivatives of pRY57 using the standard method (31). Briefly, pRY57 derivatives with the specific A6 mutations were transfected into HeLa-iA6 cells that were infected with vΔA6 virus. Recombinant viruses encoding GFP and A6 were picked under the fluorescence microscope and purified by four rounds of plaque purification on HeLa-iA6 cells, which had been grown with medium containing 100 ng/mL of tetracycline.

Plaque Formation and Growth Curve Analysis of VACV Mutants. BS-C-1 in 12-well plates was incubated with different A6 mutants for 2 h at room temperature. Following adsorption, the cells were washed twice with PBS and moved to a 37 °C incubator. For growth-curve analysis, infected cells were harvested at 0 and 24 postinfection (hpi). The viral titers in the cell lysates were determined by plaque assays on HeLa-iA6 cells that had been treated with tetracycline. For comparison of plaque morphology, medium containing 0.5% methyl cellulose was added, and plaques were visualized 48 hpi by staining the cells with crystal violet.

ACKNOWLEDGMENTS. We thank the staff of beam-line 19ID at the Advanced Photon Source for their support. This work was supported by NIH Grants AI133589 (to J.D. and Y.X.) and AI079217 (to Y.X.). J.D. is also supported by the Oklahoma Agricultural Experiment Station at Oklahoma State University under Project OKL03060.

1. Lodish H, et al. (2000) Biomembranes: Structural organizaiton and basic functions. *Molecular Cell Biology* (W. H. Freeman, New York), 4th Ed.
2. Jahn R, Lang T, Südhof TC (2003) Membrane fusion. *Cell* 112:519–533.
3. Chernomordik LV, Kozlov MM (2003) Protein-lipid interplay in fusion and fission of biological membranes. *Annu Rev Biochem* 72:175–207.
4. Shemer G, Podbilewicz B (2003) The story of cell fusion: Big lessons from little worms. *BioEssays* 25:672–682.
5. Moss B (2007) Poxviridae: The viruses and their replication. *Fields Virology*, eds Knipe DM, Howley PM (Lippincott Williams & Wilkins, Philadelphia), Vol 2, pp 2905–2946.
6. Condit RC, Moussatche N, Traktman P (2006) In a nutshell: Structure and assembly of the vaccinia virion. *Adv Virus Res* 66:31–124.
7. Moss B (2015) Poxvirus membrane biogenesis. *Virology* 479–480:619–626.
8. Weisberg AS, et al. (2017) Enigmatic origin of the poxvirus membrane from the endoplasmic reticulum shown by 3D imaging of vaccinia virus assembly mutants. *Proc Natl Acad Sci USA* 114:E11001–E11009.
9. Krijnse Locker J, Chlanda P, Sachsenheimer T, Brügger B (2013) Poxvirus membrane biogenesis: Rupture not disruption. *Cell Microbiol* 15:190–199.
10. Maruri-Avidal L, Weisberg AS, Moss B (2013) Direct formation of vaccinia virus membranes from the endoplasmic reticulum in the absence of the newly characterized L2-interacting protein A30.5. *J Virol* 87:12313–12326.
11. Kolli S, et al. (2015) Structure-function analysis of vaccinia virus H7 protein reveals a novel phosphoinositide binding fold essential for poxvirus replication. *J Virol* 89:2209–2219.
12. Wu X, et al. (2012) Vaccinia virus virion membrane biogenesis protein A11 associates with viral membranes in a manner that requires the expression of another membrane biogenesis protein, A6. *J Virol* 86:11276–11286.
13. Maruri-Avidal L, Weisberg AS, Moss B (2013) Association of the vaccinia virus A11 protein with the endoplasmic reticulum and crescent precursors of immature virions. *J Virol* 87:10195–10206.
14. Meng X, Rose L, Han Y, Deng J, Xiang Y (2017) Vaccinia virus A6 is a two-domain protein requiring a cognate N-terminal domain for full viral membrane assembly activity. *J Virol* 91:e02405-16.
15. Meng X, Embry A, Sochia D, Xiang Y (2007) Vaccinia virus A6L encodes a virion core protein required for formation of mature virion. *J Virol* 81:1433–1443.
16. Meng X, et al. (2012) Vaccinia virus A6 is essential for virion membrane biogenesis and localization of virion membrane proteins to sites of virion assembly. *J Virol* 86:5603–5613.
17. Krissinel E, Henrick K (2004) Secondary-structure matching (SSM), a new tool for fast protein structure alignment in three dimensions. *Acta Crystallogr D Biol Crystallogr* 60:2256–2268.
18. Holm L, Rosenstrom P (2010) Dali server: Conservation mapping in 3D. *Nucleic Acids Res* 38:W545–W549.
19. Lev S (2010) Non-vesicular lipid transport by lipid-transfer proteins and beyond. *Nat Rev Mol Cell Biol* 11:739–750.
20. Krumm B, Meng X, Li Y, Xiang Y, Deng J (2008) Structural basis for antagonism of human interleukin 18 by poxvirus interleukin 18-binding protein. *Proc Natl Acad Sci USA* 105:20711–20715.
21. Van Duyne GD, Standaert RF, Karplus PA, Schreiber SL, Clardy J (1993) Atomic structures of the human immunophilin FKBP-12 complexes with FK506 and rapamycin. *J Mol Biol* 229:105–124.
22. Deng J, et al. (2004) An improved protocol for rapid freezing of protein samples for long-term storage. *Acta Crystallogr D Biol Crystallogr* 60:203–204.
23. Derewenda ZS, Vekilov PG (2006) Entropy and surface engineering in protein crystallization. *Acta Crystallogr D Biol Crystallogr* 62:116–124.
24. Minor W, Cymborowski M, Otwinowski Z, Chruszcz M (2006) HKL-3000: The integration of data reduction and structure solution—From diffraction images to an initial model in minutes. *Acta Crystallogr D Biol Crystallogr* 62:859–866.
25. McCoy AJ (2007) Solving structures of protein complexes by molecular replacement with Phaser. *Acta Crystallogr D Biol Crystallogr* 63:32–41.
26. Adams PD, et al. (2010) PHENIX: A comprehensive Python-based system for macromolecular structure solution. *Acta Crystallogr D Biol Crystallogr* 66:213–221.
27. Emsley P, Cowtan K (2004) Coot: Model-building tools for molecular graphics. *Acta Crystallogr D Biol Crystallogr* 60:2126–2132.
28. Painter J, Merritt EA (2006) Optimal description of a protein structure in terms of multiple groups undergoing TLS motion. *Acta Crystallogr D Biol Crystallogr* 62:439–450.
29. DeLano WL (2002) The PyMOL molecular graphics system. Available at https://pymol.org/2/. Accessed November 2, 2017.
30. Xiao S, et al. (2010) Overexpression of Arabidopsis acyl-CoA binding protein ACBP3 promotes starvation-induced and age-dependent leaf senescence. *Plant Cell* 22:1463–1482.
31. Moss B, Earl P (1998) Overview of the vaccinia virus expression system. *Current Protocols in Molecular Biology* (John Wiley & Sons, Hoboken, NJ), p 16.16.